INTERNATIONAL JOURNAL FOR NUMERICAL METHODS IN FLUIDS, VOL. 18, 915–935 (1994)

ON THE APPROXIMATION OF HORIZONTAL GRADIENTS IN SIGMA CO-ORDINATES FOR BATHYMETRY WITH STEEP BOTTOM SLOPES

GUUS S. STELLING* AND JAN A. TH. M. VAN KESTER
Delft Hydraulics, PO Box 177, NL-2600 MH Delft, Netherlands

SUMMARY

Nowadays the simulation of free surface flow and transport in rivers, estuaries and seas is often based upon three-dimensional modelling systems. Most of these three-dimensional modelling systems use sigma co-ordinates in the vertical. By the use of the sigma transformation the water column can be divided into the same number of layers independently of the water depth. Especially for steep bottom slopes combined with vertical stratification of the density, sigma-transformed grids impose numerical problems for the accurate approximation of horizontal gradients. This paper deals with algorithms for the approximation in sigma co-ordinates of the horizontal diffusive fluxes of temperature and salinity and for the approximation of the horizontal pressure gradients. The approximation of the horizontal diffusive fluxes is based upon a finite volume method. The approximation of the pressure gradients is directly related to the approximation of the diffusive fluxes. Artificial vertical diffusion and artificial flow due to truncation errors are minimized. The method described in this paper is not hampered by the so-called 'hydrostatic consistency condition'. This will be illustrated by numerical experiments.

KEY WORDS Three-dimensional modelling systems Shallow water Sigma co-ordinates Diffusive flux Pressure gradient Artificial vertical transport Artificial flow Hydrostatic consistency.

1. INTRODUCTION

Nowadays the simulation of free surface flow and transport in rivers, estuaries and seas is often based upon three-dimensional modelling systems. Most of these three-dimensional modelling systems use sigma co-ordinates for the numerical approximation in the vertical. By the use of the sigma transformation the water column is divided into the same number of layers independently of the water depth. This leads to a smooth representation of the topography instead of the 'staircase' grid obtained with Cartesian co-ordinates.

However, sigma-transformed grids impose numerical problems for the accurate approximation of horizontal gradients in the case of stratified flow over steep topography.[1] This may lead to the conclusion that sigma co-ordinates are not acceptable for estuary models[2] because of unrealistic mixing.

Estuaries are sometimes defined as in interface between salt and fresh water (see e.g. Reference 3). Generally in an estuary the bottom is strongly variable. There may be a transition from deep channels to shallow tidal flat areas. To model the physical processes in estuaries, a three-dimensional hydrodynamic modelling system should include density effects in the momentum equations and should also include transport equations for salt, heat, turbulent kinetic energy,

* also at: Delft University of Technology, PO Box 5048, NL-2600 VA Delft, Netherlands

CCC 0271–2091/94/100915–21

Received April 1993
Revised November 1993

etc. In the vertical momentum equation the vertical accelerations are neglected, which leads to the hydrostatic pressure equation. Vertical velocities are computed from the continuity equation.

The modelling of flow and transport is often based upon the following set of equations given in Cartesian co-ordinates:

continuity equation,

$$\nabla \cdot \mathbf{u} = 0; \tag{1a}$$

momentum equations in horizontal direction,

$$\frac{\mathrm{D}u_i}{\mathrm{D}t} + \frac{1}{\rho_0}\frac{\partial p}{\partial x_i} = \frac{1}{\rho_0}\frac{\partial \tau_{i,j}}{\partial x_j}, \quad i = 1, 2, \quad j = 1, 2, 3; \tag{1b}$$

hydrostatic pressure equation,

$$\frac{\partial p}{\partial x_3} = -\rho g; \tag{1c}$$

transport equations,

$$\frac{\partial c_l}{\partial t} + \nabla \cdot \mathbf{F}_l = 0, \quad l = 1, \ldots, l_c; \tag{1d}$$

where u_i is the velocity in the x_i-direction, p is the pressure, ρ is the density, ρ_0 is the reference density, c_l is the concentration of scalar quantities (e.g. salinity and temperature), $\mathbf{F}$ is the concentration flux due to advection and diffusion and $\tau_{i,j}$ is the shear stress computed by some turbulence closure model ($\mathrm{D}u_i/\mathrm{D}t = \partial u_i/\partial t + u_j\, \partial u_i/\partial x_j$, where the summation convention is used).

We will also use the following notation: $u = u_1$, $v = u_2$, $w = u_3$, $x = x_1$, $y = x_2$, $z = x_3$. The vertical co-ordinate z is bounded by

$$-d(x, y) \leqslant z \leqslant \zeta(x, y, t),$$

where d is the depth below some plane of reference and ζ is the water level above some plane of reference.

The density ρ follows from an equation of state given by

$$\rho = \rho(s, T),$$

where s is the salinity and T is the temperature.

In the next section sigma co-ordinates are introduced and some of the difficulties in the use of sigma grids near steep bottom slopes are discussed. Section 3 concerns the transport equation in sigma co-ordinates. A new algorithm for the accurate approximation of the horizontal diffusive fluxes is introduced. Section 4 deals with the approximation of the horizontal pressure gradient in the momentum equation. The relation between gradient fluxes in the transport equation and the contribution to the pressure gradient resulting from density differences will be shown. In Section 5 the numerical results for three test problems are described. Section 6 contains some concluding remarks.

2. SIGMA CO-ORDINATES

In three-dimensional shallow water models a sigma co-ordinate transformation is often applied.[4] For an elaborate discussion on the advantages and disadvantages of this approach, see

Reference 5. In our opinion the main advantage of this co-ordinate system is the fact that it is fitted to both the moving free surface and the bottom topography. This is essential for the accurate approximation of the vertical flow distribution without a large number of vertical grid points. Moreover, these 'terrain-following co-ordinates' allow an efficient grid refinement near the free surface (in the case of wind-driven flow) and near the bed.

In this paper the sigma co-ordinate system is defined as

$$x^* = x, \qquad y^* = y, \qquad \sigma = \frac{z - \zeta}{H}, \qquad t^* = t,$$

where $H = \zeta + d$ is the total water depth, $z = \zeta(x, y, t)$ or $\sigma = 0$ at the free water surface and $z = -d(x, y)$ or $\sigma = -1$ at the bottom.

The derivatives in the original Cartesian co-ordinate system are expressed in σ-co-ordinates by the chain rule

$$\frac{\partial}{\partial t} = \frac{\partial}{\partial t^*} + \frac{\partial \sigma}{\partial t}\frac{\partial}{\partial \sigma},$$

$$\frac{\partial}{\partial x_i} = \frac{\partial}{\partial x_i^*} + \frac{\partial \sigma}{\partial x_i}\frac{\partial}{\partial \sigma}, \quad i = 1, 2,$$

$$\frac{\partial}{\partial x_3} = \frac{1}{H}\frac{\partial}{\partial \sigma}$$

and substituted into (1).

The velocities u_i^*, $i = 1, 2, 3$, are defined by

$$u_i^* = u_i, \quad i = 1, 2, \qquad u_3^* = \omega = H\frac{\mathrm{D}\sigma}{\mathrm{D}t}.$$

The velocities u_1^* and u_2^* remain the strictly horizontal components of the velocity vector.

The system of equations (1) becomes:

continuity equation,

$$\frac{\partial \zeta}{\partial t^*} + \frac{\partial (Hu^*)}{\partial x^*} + \frac{\partial (Hv^*)}{\partial y^*} + \frac{\partial \omega}{\partial \sigma} = 0; \tag{2a}$$

momentum equations,

$$\frac{\mathrm{D}u_i^*}{\mathrm{D}t^*} + \frac{1}{\rho_0}\left(\frac{\partial p^*}{\partial x_i^*} + \frac{\partial \sigma}{\partial x_i}\frac{\partial p^*}{\partial \sigma}\right) = \frac{1}{\rho_0}\frac{\partial \tau_{i,j}^*}{\partial x_j^*}; \tag{2b}$$

hydrostatic pressure equation,

$$\frac{\partial p^*}{\partial \sigma} = -\rho g H; \tag{2c}$$

transport equations,

$$\frac{\partial c_l^*}{\partial t^*} + \nabla^* \cdot \mathbf{F}_l^* = 0; \tag{2d}$$

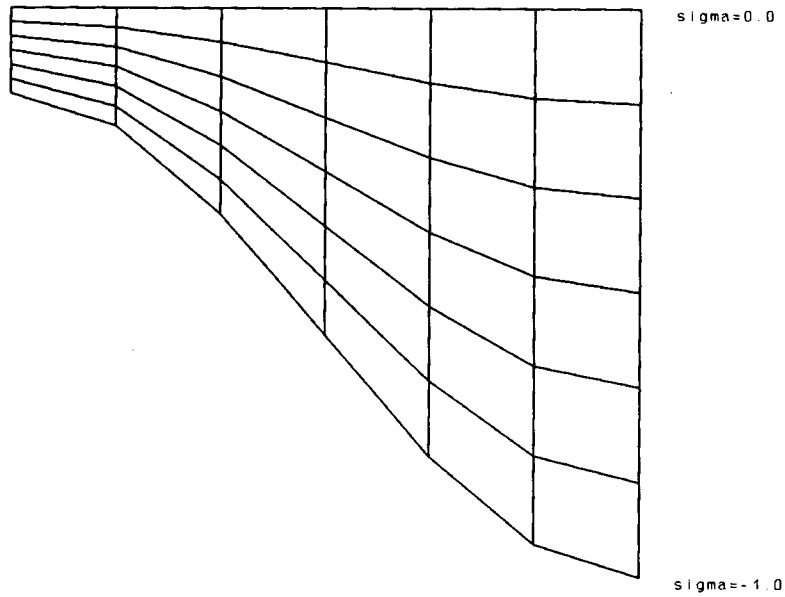

Figure 1. The σ-grid

where

$$\frac{Du_i^*}{Dt^*} = \frac{\partial u_i^*}{\partial t^*} + u^* \frac{\partial u_i^*}{\partial x^*} + v^* \frac{\partial u_i^*}{\partial y^*} + \frac{\omega}{H} \frac{\partial u_i^*}{\partial \sigma}.$$

It should be noted that the turbulent closure models for $\partial \tau_{i,j}^*/\partial x_j^*$ are not necessarily an exact transformation of $\partial \tau_{i,j}/\partial x_j$. Sometimes they are reformulated within the framework of the transformed co-ordinates.[6]

For numerical approximation a grid has to be defined. Owing to the σ-transformation, this grid is fitted to the free surface and the bottom. In estuaries such a grid may deteriorate quite strongly in the presence of steep bottom slopes and shallow areas, e.g. near tidal flats (see Figure 1). Grids of this type cause problems when computing horizontal gradients, as has been recognized by several authors (see e.g. References 1, 2, 5 and 7–9).

We consider the transformation of the horizontal pressure gradient as follows:

$$\frac{\partial p}{\partial x} = \frac{\partial p^*}{\partial x^*} + \frac{\partial \sigma}{\partial x} \frac{\partial p^*}{\partial \sigma} = \frac{\partial p^*}{\partial x^*} - \frac{1}{H} \left(\frac{\partial \zeta}{\partial x} + \sigma \frac{\partial H}{\partial x} \right) \frac{\partial p^*}{\partial \sigma}.$$

Near steep bottom slopes small pressure gradients might be the result of the sum of two relatively large terms of opposite sign. Small truncation errors in the approximation of both terms result in a relatively large error in the pressure gradient. This might produce artificial flow. Observations of this kind have led to the notion of 'hydrostatic consistency' (see e.g. Reference 8). In the notation used by Haney[1] this consistency relation is given by

$$\left| \frac{\sigma}{H} \frac{\partial H}{\partial x} \right| \Delta x < \Delta \sigma,$$

where Δx and $\Delta \sigma$ are grid sizes. If this relation is not satisfied, then a numerical scheme might

be non-convergent. However, in estuaries, tidal flats are characterized by $H \to 0$, which means that convergence might become impossible.

In the case of steep bottom slopes there are similar difficulties in the approximation of the horizontal gradient transport of matter, such as salinity and heat.

3. APPROXIMATION OF DIFFUSIVE FLUXES

The fluxes of the transport equations (1d) consist of both advective and diffusive fluxes. In sigma co-ordinates the approximation of the advective fluxes does not introduce large truncation errors. Therefore in this section we consider only diffusive fluxes given by

$$F_i = D_H \frac{\partial c}{\partial x_i}, \quad i = 1, 2, \qquad F_3 = D_V \frac{\partial c}{\partial x_3},$$

where D_H denotes the horizontal eddy diffusion coefficient and D_V denotes the vertical eddy diffusion coefficient. The vertical eddy diffusion coefficient is determined by a turbulence closure scheme. The horizontal eddy diffusion coefficient depends on the horizontal grid resolution and is usually an order of magnitude larger.

Transformation of the horizontal diffusion terms to x^*, y^*, σ, t^* is a tedious task, leading by the chain rule to various cross-derivatives. For example, the transformation of a simple second-order derivative leads to

$$\frac{\partial^2 c}{\partial x^2} = \frac{\partial^2 c^*}{\partial x^{*2}} + \left(\frac{\partial \sigma}{\partial x}\right)^2 \frac{\partial^2 c^*}{\partial \sigma^2} + 2 \frac{\partial \sigma}{\partial x} \frac{\partial^2 c^*}{\partial x^* \partial \sigma} + \frac{\partial^2 \sigma}{\partial x^2} \frac{\partial c^*}{\partial \sigma}.$$

For such a combination of terms it is difficult to find a numerical approximation that is stable and positive. Near steep bottom slopes or near tidal flats where the total depth becomes very small, truncations errors in the approximation of the horizontal diffusive fluxes in σ-co-ordinates are likely to become very large, similarly to the horizontal pressure gradient. Some authors[6] omit several terms of the transformation, yielding the following diffusive fluxes:

$$F_1^* = D_H \frac{\partial c^*}{\partial x^*}, \qquad F_2^* = D_H \frac{\partial c^*}{\partial y^*}, \qquad F_3^* = \frac{D_V}{H} \frac{\partial c^*}{\partial \sigma}. \tag{3}$$

The physical conditions (upwelling) which cause this new formulation to give a better description of the transport process are certainly not fulfilled in many estuaries. If we omit vertical diffusion, then this new formulation will still cause some numerical vertical diffusion, especially near steep bottom slopes or near tidal flats. Owing to this phenomenon, it will be difficult to simulate the stratification of a salt wedge in an estuary very accurately. Thus the complete transformation must be included. However, in that case numerical problems are encountered concerning accuracy, stability and monotonicity. In this section a method is introduced which gives a consistent, stable and monotonic approximation of the horizontal diffusion terms even when the hydrostatic consistency condition is violated. The method is based upon a finite volume method.

3.1. A finite volume method for a σ-grid

Description of the algorithm. Finite volume methods[10–12] are commonly used for the approximation of systems of conservation laws. They yield conservative approximations for arbitrary grids without the need for explicit analytic transformation of Cartesian equations. In

general, a finite volume method is based upon integration of the transport equation, given in Cartesian co-ordinates, over a control volume combined with the Gauss theorem. The Gauss theorem is given by

$$\int_v \nabla \cdot \mathbf{F} \, dv = \oint_s \mathbf{F} \cdot \mathbf{n} \, ds,$$

where $\mathbf{n}$ denotes the normal to the boundary. Applied to equation (1d), this yields

$$\int_v \frac{\partial c}{\partial t} \, dv + \oint_s \mathbf{F} \cdot \mathbf{n} \, ds = 0.$$

Taking into account that the control volume is time-variable, as in the case of σ-co-ordinates, this equation can be written as

$$\frac{\partial}{\partial t} \int_v c \, dv + \oint_s \mathbf{F} \cdot \mathbf{n} \, ds = \oint_s c \frac{\partial n}{\partial t} \, ds.$$

The right-hand side of this equation describes some pseudo-advection due to the displacement of the vertical walls of the control volume. In σ-co-ordinates this is taken into account by the definition of ω. The fluxes of this equation can be added together to yield a new flux $\mathbf{F}^*$. After dropping the asterisk, we obtain

$$\frac{\partial}{\partial t} \int_v c \, dv + \oint_s \mathbf{F} \cdot \mathbf{n} \, ds = 0. \tag{4}$$

Instead of transforming the transport equation to σ-co-ordinates, we generate a sigma grid by choosing a distribution of the vertical co-ordinate sigma:

$$\{\sigma_k | k = 0, \ldots, K\}, \qquad \sigma_K = 0, \qquad \sigma_0 = -1,$$

where K is the number of layers.

Consider the sigma grid lines as the boundaries of the time-varying control volumes in Cartesian co-ordinates. In this way we obtain finite volumes as given by Figure 2.

The direction of the vertical grid lines is such that the vertical diffusive fluxes are straightforward to implement. The only true difficulty is the approximation of the horizontal diffusive fluxes. For that purpose a special method is constructed. To explain this method, it is sufficient to consider a simplified two-dimensional transport equation

$$\frac{\partial c(x, z, t)}{\partial t} - \frac{\partial}{\partial x} D_H \frac{\partial c(x, z, t)}{\partial x} = 0. \tag{5}$$

We use cell-centred finite volumes. This means that the numerical values $c_{i,k}$ are located at the cell centres as given by Figure 2. For the simplified diffusion equation and for the cell-centred

* This relation can be proved by repeated application of the Leibnitz integration rule, which is given by

$$\frac{\partial}{\partial x} \int_{\alpha(x)}^{\beta(x)} \phi(x, y) \, dy = \int_{\alpha(x)}^{\beta(x)} \frac{\partial}{\partial x} \phi(x, y) \, dy + \phi(x, \beta) \frac{\partial \beta}{\partial x} - \phi(x, \alpha) \frac{\partial \alpha}{\partial x}.$$

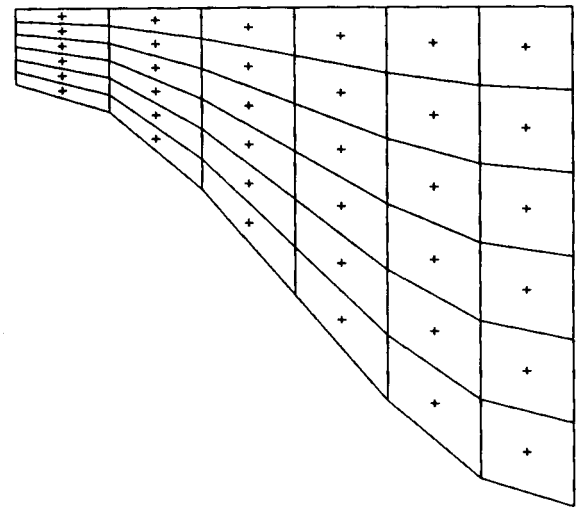

Figure 2. Cell-centred control volumes

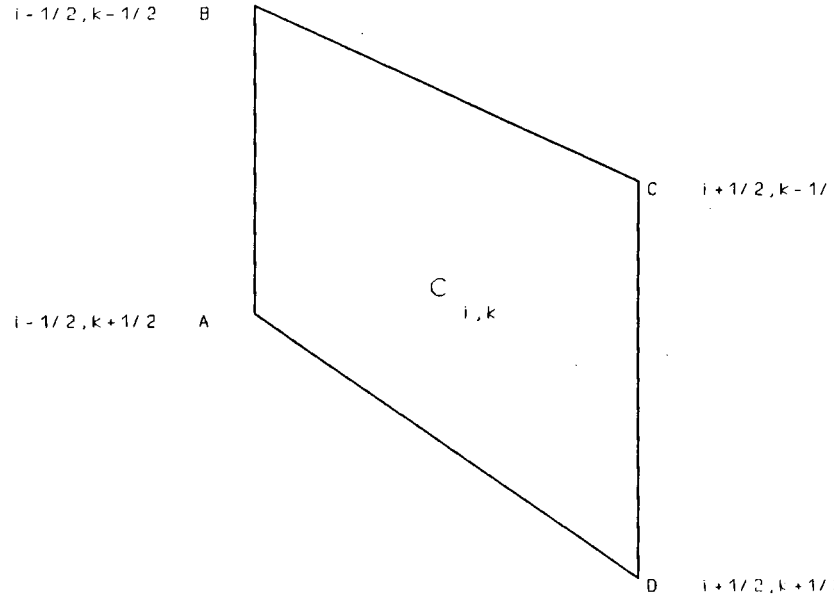

Figure 3. Cell numbering

volume given by Figure 3, the finite volume method implies a numerical approximation of the following integrals:

$$\frac{\partial}{\partial t}\iint_{ABCD} c\,dx\,dz + \int_{x_A, x_A}^{x_B, z_B} D_H \frac{\partial c}{\partial x} dz + \int_{x_B, z_B}^{x_C, z_C} D_H \frac{\partial c}{\partial x} dz + \int_{x_C, z_C}^{x_D, z_D} D_H \frac{\partial c}{\partial x} dz + \int_{x_D, z_D}^{x_A, z_A} D_H \frac{\partial c}{\partial x} dz = 0. \tag{6}$$

For this equation a finite volume method has to be constructed that meets the following

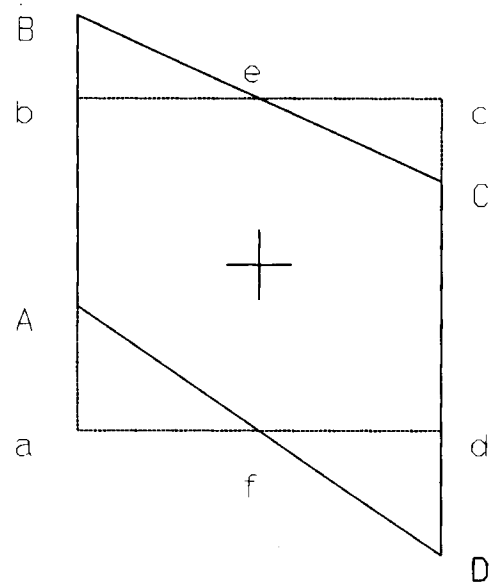

Figure 4. Control volume for diffusive fluxes

requirements: (i) consistent approximation of the horizontal diffusive fluxes; (ii) fulfilment of the min–max principle; (iii) minimal artificial vertical diffusion.

For the discretization of (5) approximations of $\partial c/\partial x$ have to be given at the side walls of the control volume. For this aim we consider in Figure 4 the points a–f, where

$$x_a = x_A, \qquad z_a = (z_A + z_D)/2,$$

$$x_b = x_B, \qquad z_b = (z_B + z_C)/2,$$

$$x_c = x_C, \qquad z_c = (z_B + z_C)/2,$$

$$x_d = x_D, \qquad z_d = (z_A + z_D)/2,$$

$$x_e = (x_A + x_D)/2, \qquad z_e = (z_A + z_D)/2,$$

$$x_f = (x_B + x_C)/2, \qquad z_f = (z_B + z_C)/2.$$

If in the interval $[(x_e, z_e), (x_B, x_B)]$ the same numerical approximation for $\partial c/\partial x$ is used as in the interval $[(x_B, z_B), (x_b, z_b)]$, then the integral along these two intervals is zero. The same result can be obtained along the intervals $[(x_e, z_e), (x_C, z_C)]$ and $[(x_c, z_c), (x_C, z_C)]$. By the same argument one can assume that in the intervals $[(x_A, z_A), (x_f, z_f)]$ and $[(x_D, z_D), (x_d, z_d)]$ the integrals are the same. On the basis of these assumptions one can show that a consistent, semi discrete approximation of equation (6) is given by

$$(x_d - x_a)(z_b - z_a)\frac{dc_{i,k}}{dt} = -\int_{x_a, z_a}^{x_b, z_b} D_H \frac{\partial c}{\partial x}\, dz - \int_{x_c, z_c}^{x_d, z_d} D_H \frac{\partial c}{\partial x}\, dz. \tag{7}$$

The time derivative on the left-hand side of this equation can be approximated by any time integration method (see e.g. Reference 13). We will use Euler's explicit method.

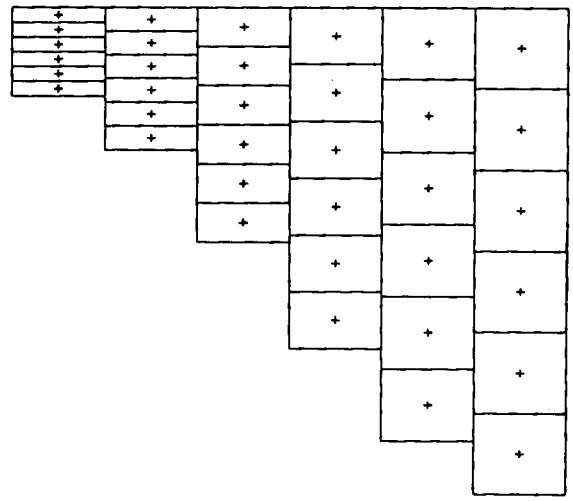

Figure 5. Control volumes for diffusive fluxes

For the right-hand side one must realize that cells of shape abcd might have more than two adjacent cells in the horizontal direction (see Figure 5). For the approximation of the right-hand side of equation (7) an interval

$$[\min(-d_i, -d_{i+1}), \max(\zeta_i, \zeta_{i+1})]$$

between two vertical columns of control volumes is divided into $2K + 1$ subintervals

$$[z_{i+1/2,l}, z_{i+1/2,l+1}], \quad l = 0, \ldots, 2K, \qquad z_0 = \min(-d_i, -d_{i+1}), \qquad z_{2K+1} = \max(\zeta_i, \zeta_{i+1}).$$

The set of points $\{z_{i+1/2,0}, \ldots, z_{i+1/2,2K+1}\}$ is ordered such that

$$z_{i+1/2,l+1} \geqslant z_{i+1/2,l} \quad \text{for } l = 0, \ldots, 2K.$$

This set results from a sort–merge operation of the two sets

$$\{\zeta_i + \sigma_k H_i | k = 0, \ldots, K\}, \qquad \{\zeta_{i+1} + \sigma_k H_{i+1} | k = 0, \ldots, K\}, \qquad \sigma_K = 0, \qquad \sigma_0 = -1.$$

To each interval $[z_{i+1/2,l}, z_{i+1/2,l+1}]$ one or two adjacent cells are connected with cell-centred concentrations $c_{i,m(l)}$ and $c_{i+1,n(l)}$. Here $m(l)$ and $n(l)$ denote cell numbers. In extreme cases, such as in the case of cells neighbouring tidal flats, $m(l)$ or $n(l)$ only contains the number of the cell of the top layer. If there is only one cell connected to an interval, as might happen near the bottom or near the free surface, then the diffusive flux is assumed to be zero (see Figure 5). It also follows from Figure 5 that adjacency of control volumes is not according to grid lines of constant σ but according to the smallest possible difference in the vertical co-ordinates. Adjacency is no longer a one-to-one relation, since one cell might be adjacent to various cells.

For adjacent cells the mutual diffusive flux must be approximated. A straightforward approach would be to approximate $\partial c/\partial x$ in the centre of the mutual interval $[z_{i+1/2,l}, z_{i+1/2,l+1}]$, denoted by $z_{i+1/2,l+1/2}$, as

$$\frac{\partial c(x_{i+1/2}, z_{i+1/2,l+1/2})}{\partial x} \approx \frac{c_{i+1}(z_{i+1/2,l+1/2}) - c_i(z_{i+1/2,l+1/2})}{x_{i+1} - x_i}, \tag{8}$$

where $c_i(z)$ denotes some interpolation function that interpolates between the values $c_{i,1}, \ldots, c_{i,K}$. As interpolation function one can use Lagrangian or Hermitian interpolation functions of any order. However, this approach, as was shown by numerical experiments, has the following disadvantages: (i) no guaranteed fulfilment of the min–max principle; (ii) a slight (depending on the order of the interpolation function) but persistent artificial vertical diffusion in all cases except for a linear vertical distribution of the concentration.

To circumvent these disadvantages, a non-linear approach is chosen which consists of the following steps.

Step 1

First, diffusive fluxes $f_{i+1/2,l+1/2}$, $l = 0, \ldots, 2K$, are defined according to

$$f_{i+1/2,l+1/2} = \begin{cases} D_H \min(\Delta_m c, \Delta_n c) \dfrac{z_{i+1/2,l+1} - z_{i+1/2,l}}{x_{i+1} - x_i}, & \Delta_m c > 0 \wedge \Delta_n c > 0, \\ D_H \max(\Delta_m c, \Delta_n c) \dfrac{z_{i+1/2,l+1} - z_{i+1/2,l}}{x_{i+1} - x_i}, & \Delta_m c \leqslant 0 \wedge \Delta_n c \leqslant 0, \\ 0, & \Delta c_m \Delta_n c < 0. \end{cases} \tag{9}$$

The differences $\Delta_{m/n} c = \Delta_{m/n} c_{i+1/2,l+1/2}$ are given by

$$\left.\begin{aligned} \Delta_m c_{i+1/2,l+1/2} &= c_{i+1}(z_{i,m(l)}) - c_{i,m(l)} \\ \Delta_n c_{i+1/2,l+1/2} &= c_{i+1,n(l)} - c_i(z_{i+1,n(l)}) \end{aligned}\right\} \quad l = 0, \ldots, 2K, \tag{10}$$

where $c_i(z)$ is a simple linear interpolation formula given by

$$c_i(z) = \begin{cases} c_{i,1}, & z \leqslant z_{i,1}, \\ \dfrac{z - z_{i,k}}{z_{i,k+1} - z_{i,k}} c_{i,k+1} + \dfrac{z_{i,k+1} - z}{z_{i,k+1} - z_{i,k}} c_{i,k}, & z_{i,k} < z \leqslant z_{i,k+1}, \\ c_{i,K}, & z \geqslant z_{i,K}. \end{cases} \tag{11}$$

The coefficients of this interpolation formula are always positive and less than or equal to one. The two possible stencils for the finite difference approximation of the horizontal gradient are shown in Figure 6.

Step 2

In this step the diffusive fluxes are added to the appropriate control volumes according to

$$V_{i,k}^{\tau+1} c_{i,k}^{\tau+1} = V_{i,k}^{\tau} c_{i,k}^{\tau} - \Delta t \sum_{\forall l \mid m(l) = k} f_{i+1/2,l+1/2}^{\tau} + \Delta t \sum_{\forall l \mid n(l) = k} f_{i-1/2,l+1/2}^{\tau}, \tag{12}$$

where τ is the time index, $t = \tau \Delta t$ and V^{τ} denotes the size of the control volume. The absence of advection implies $V^{\tau} = V^{\tau+1}$.

Consistency of diffusive fluxes. For a finite volume method for diffusion problems a consistent approximation of the diffusive fluxes is a necessary condition. Obviously this condition is equivalent to the condition that $\partial c/\partial x$ must be approximated consistently in the intervals $(z_{i+1/2,l}, z_{i+1/2,l+1})$, $l = 0, \ldots 2K$.

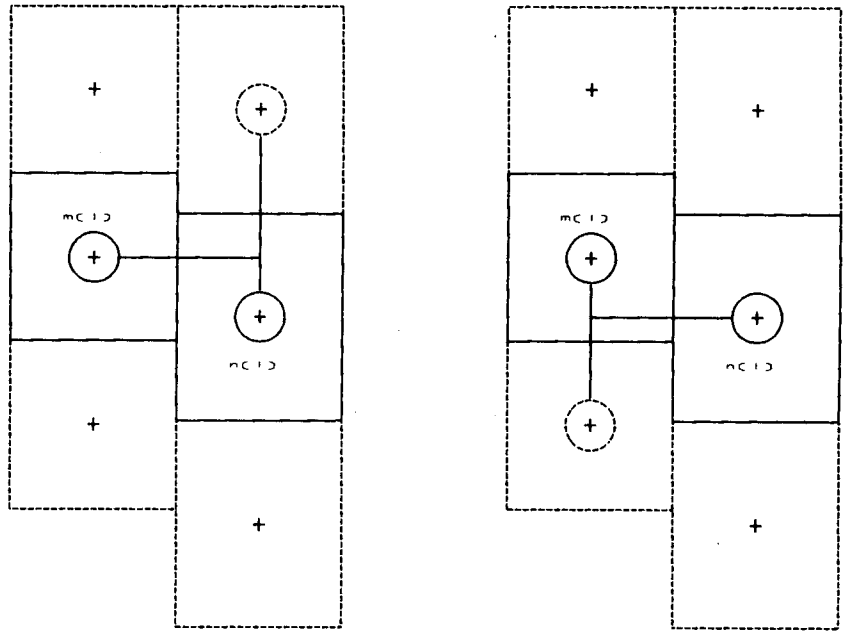

Figure 6. Stencils for diffusive fluxes

Before proving consistency, we define the values Δz and Δx as

$$\Delta z = \max_{\forall i,k} |z_{i,k+1} - z_{i,k}|, \qquad \Delta x = \max_{\forall i} |x_{i+1} - x_i|.$$

Equation (9) implies

$$\frac{\partial c(x_{i+1/2}, z_{i,m(l)})}{\partial x} = \frac{\Delta_m c_{i+1/2,l+1/2}}{x_{i+1} - x_i} + O(\Delta x, \Delta z^2),$$

$$\frac{\partial c(x_{i+1/2}, z_{i,n(l)})}{\partial x} = \frac{\Delta_n c_{i+1/2,l+1/2}}{x_{i+1} - x_i} + O(\Delta x, \Delta z^2).$$

From Figure 6 it follows that $|z_{i,m(l)} - z_{i+1,n(l)}| \leqslant \Delta z$ and $z_{i,m(l)} \leqslant z_{i+1/2,l+1/2} \leqslant z_{i+1,n(l)}$ or $z_{i,m(l)} \geqslant z_{i+1/2,l+1/2} \geqslant z_{i+1,n(l)}$, so

$$\frac{\partial c(x_{i+1/2}, z_{i+1/2,l+1/2})}{\partial x} = \frac{\Delta_m c_{i+1/2,l+1/2}}{x_{i+1} - x_i} + O(\Delta x, \Delta z),$$

$$\frac{\partial c(x_{i+1/2}, z_{i+1/2,l+1/2})}{\partial x} = \frac{\Delta_n c_{i+1/2,l+1/2}}{x_{i+1} - x_i} + O(\Delta x, \Delta z).$$

From this it follows that the first two possibilities of equation (9) are indeed consistent approximations of the diffusive fluxes. The third possibility means a zero flux in the case of gradients of opposite sign at both ends of the interval $[z_{i,m(l)}, z_{i,n(l)}]$. Because of this change in sign, a zero flux is also a consistent approximation in this interval. This means that equation (9) gives at least a first-order-consistent approximation.

Min–max condition. The min–max condition (see e.g. Reference 14) implies the following:

$$\min_{\forall i,k}(c_{i,k}^{\tau}) \leqslant c_{i,k}^{\tau+1} \leqslant \max_{\forall i,k}(c_{i,k}^{\tau}) \quad \forall i, k.$$

This is a necessary condition to get numerical solutions that are physically acceptable. Especially for the numerical implementation of diffusion this is important, since the physical nature of diffusion implies reduction of the gradients and not amplification.

In the following we will show that the algorithm given by equations (9)–(12) fulfils this condition. For $c^{\tau+1}$ the following inequality holds:

$$c_{i,k}^{\tau+1} \geqslant c_{i,k}^{\tau} + \frac{\Delta t}{V_{i,k}}\left(-\sum_{\forall l \mid m(l)=k \wedge f>0} f_{i+1/2,l+1/2}^{\tau} + \sum_{\forall l \mid n(l)=k \wedge f<0} f_{i-1/2,l+1/2}^{\tau}\right).$$

From this relation and equation (9) the following inequality follows:

$$c_{i,k}^{\tau+1} \geqslant c_{i,k}^{\tau} + \frac{\Delta t}{V_{i,k}}\left(-\sum_{\forall l \mid m(l)=k \wedge f>0} D_{\mathrm{H}} \frac{\Delta_m c_{i+1/2,l}^{\tau} \Delta z_{i+1/2,l}}{\Delta x_{i+1/2}} + \sum_{\forall l \mid n(l)=k \wedge f<0} D_{\mathrm{H}} \frac{\Delta_n c_{i-1/2,l}^{\tau} \Delta z_{i-1/2,l}}{\Delta x_{i-1/2}}\right).$$

This inequality can be rewritten as

$$c_{i,k}^{\tau+1} \geqslant (1 - \Delta t \alpha_{i,k}) c_{i,k}^{\tau} + \Delta t \sum_{l=1}^{K} \beta_{i,k,l} c_{i-1,l}^{\tau} + \Delta t \sum_{l=1}^{K} \gamma_{i,k,l} c_{i+1,l}^{\tau},$$

where α, β and γ are coefficients that are zero or positive as follows from equations (10) and (11). These equations also yield the following:

$$\alpha_{i,k} + \sum_{l=1}^{K} \beta_{i,k,l} + \sum_{l=1}^{K} \gamma_{i,k,l} = 0.$$

Now it follows that if

$$\Delta t \alpha_{i,j} \leqslant 1 \quad \forall i, j, \tag{13}$$

then

$$c_{i,k}^{\tau+1} \geqslant \min(c_{i,k}^{\tau}) \quad \forall i, k.$$

In a similar way one can prove that

$$c_{i,k}^{\tau+1} \leqslant \max(c_{i,k}^{\tau}) \quad \forall i, k.$$

The proof of this maximum principle starts with the observation that

$$c_{i,k}^{\tau+1} \leqslant c_{i,k}^{\tau} - \frac{\Delta t}{V_{i,k}}\left(\sum_{\forall l \mid m(l)=k \wedge f<0} f_{i+1/2,l+1/2}^{\tau} - \sum_{\forall l \mid n(l)=k \wedge f>0} f_{i-1/2,l+1/2}^{\tau}\right),$$

after which the proof is completely analogous. Again also condition (13) must be fulfilled. Note that in case of a constant horizontal grid size Δx and a constant horizontal diffusion D_{H} this condition is always fulfilled if

$$D_{\mathrm{H}} \Delta t / \Delta x^2 \leqslant \tfrac{1}{2} \tag{14}$$

This is the usual stability condition for explicit approximations of a one-dimensional diffusion equation. Obviously the min–max condition is a sufficient condition for stability.

4. APPROXIMATION OF THE PRESSURE TERM

This section deals with the approximation of the horizontal gradient of the pressure, $\partial p/\partial x$, in equation (1). For this approximation we assume a staggered grid as shown in Figure 7.

The horizontal gradients of the pressure must be approximated for the horizontal momentum equations. From Figure 7 it follows that the pressure gradient must be computed along the same verticals as the horizontal concentration gradients. The pressure p in Cartesian co-ordinates is given by

$$p(x, z, t) = \int_{z'=z}^{\zeta} \rho(x, z', t) g \, dz'.$$

From the Leibnitz rule it follows that $\partial p/\partial x$ is given by

$$\frac{\partial}{\partial x} p(x, z) = \frac{\partial}{\partial x} \int_{z'=z}^{\zeta(x)} \rho(x, z') g \, dz' = \int_{z'=z}^{\zeta(x)} g \frac{\partial}{\partial x} \rho(x, z') \, dz' + g\rho(\zeta) \frac{\partial \zeta}{\partial x}. \tag{15}$$

The relation between the density ρ and the salinity s and temperature T is given by the equation of state

$$\rho = \rho(s(x, t), T(x, t)).$$

It follows that

$$\frac{\partial \rho}{\partial x} = \frac{\partial \rho}{\partial s} \frac{\partial s}{\partial x} + \frac{\partial \rho}{\partial T} \frac{\partial T}{\partial x}.$$

If the horizontal gradients of the concentrations are zero, then there is no contribution of the horizontal density gradients to the driving force in the momentum equation. It is important to have exactly the same mechanism in the numerical approximation. *This means that if the*

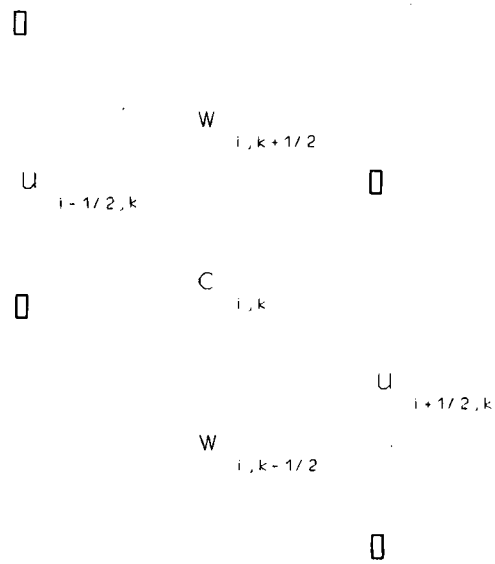

Figure 7. Staggered grid for σ-co-ordinates in physical space

horizontal gradients used in the transport equation are zero, then the horizontal gradients of the pressure should be zero too. If not, then there will always be artificial flow near steep bottom slopes owing to truncation errors. Therefore the procedure described in Section 3 will also be used for the approximation of $\partial p/\partial x$; in other words, the numerical approximations for the horizontal concentration gradients will be used for the approximation of the pressure gradients.

The integral in equation (15) is replaced by a summation over the intervals which are in the water column above the velocity point with vertical co-ordinate z. In this way we obtain the following approximation of equation (15):

$$\left(\frac{\partial p}{\partial x}\right)(x_{i+1/2}, z) = g \sum_{l=\kappa+1}^{2K+1} \left[\left(\frac{\partial \rho}{\partial s}\right)_{i+1/2,l+1/2} \frac{f_{i+1/2,l+1/2}(s)}{D_H} + \left(\frac{\partial \rho}{\partial T}\right)_{i+1/2,l+1/2} \frac{f_{i+1/2,l+1/2}(T)}{D_H}\right]$$
$$+ g \frac{z_{i+1/2,\kappa+1} - z}{z_{i+1/2,\kappa+1} - z_{i+1/2,\kappa}} \left[\left(\frac{\partial \rho}{\partial s}\right)_{i+1/2,\kappa+1/2} \frac{f_{i+1/2,\kappa+1/2}(s)}{D_H} + \left(\frac{\partial \rho}{\partial T}\right)_{i+1/2,\kappa+1/2} \frac{f_{i+1/2,\kappa+1/2}(T)}{D_H}\right]$$
$$+ g\rho \frac{\zeta_{i+1} - \zeta_i}{\Delta x}, \tag{16}$$

where

$$\kappa = \max\{l | z_{i+1/2,l} < z\}.$$

Obviously, when equation (16) is applied, then zero horizontal gradients of salinity and temperature imply zero density gradients, so artificial upwelling is minimized. A density field which is physically in equilibrium will remain in equilibrium. This observation will be illustrated in the next section. Note that this approximation implies that sigma transformation is taken into account implicitly and at the numerical level rather than by explicit and analytic transformation of equation (15). This approach is similar to the finite volume approach for diffusion; in other words, *for convergence this approach does not have to satisfy the hydrostatic consistency condition.*

5. TEST PROBLEMS

In this section three test problems will be considered. The first test problem deals with a horizontal diffusion problem. The second example illustrates the horizontal pressure computation proposed in this paper. These two examples are two-dimensional lateral-averaged. The third example consists of a three-dimensional diffusion problem.

The first test problem deals with a simple diffusion equation given by equation (5). The bathymetry (see Figure 8) is given by $0 \leqslant x \leqslant 100$ m and $-x/10 - 1 \leqslant z \leqslant 0$. The boundaries at $x = 0$ and 100 are closed. Here zero diffusive fluxes are prescribed at the boundaries. The initial condition is given by

$$c = \begin{cases} 0{\cdot}0\ \mathrm{kg\,m^{-3}} & \text{for } z \geqslant -5\ \mathrm{m}, \\ 30{\cdot}0\ \mathrm{kg\,m^{-3}} & \text{for } z < -5\ \mathrm{m}. \end{cases}$$

Vertical diffusion is assumed to be zero. The horizontal diffusion coefficient D_H is set at 10 $\mathrm{m^2\,s^{-1}}$. The initial condition is an equilibrium solution and so also is the steady state solution. For the numerical approximation we use a sigma grid with 10 × 10 grid cells. The initial condition is

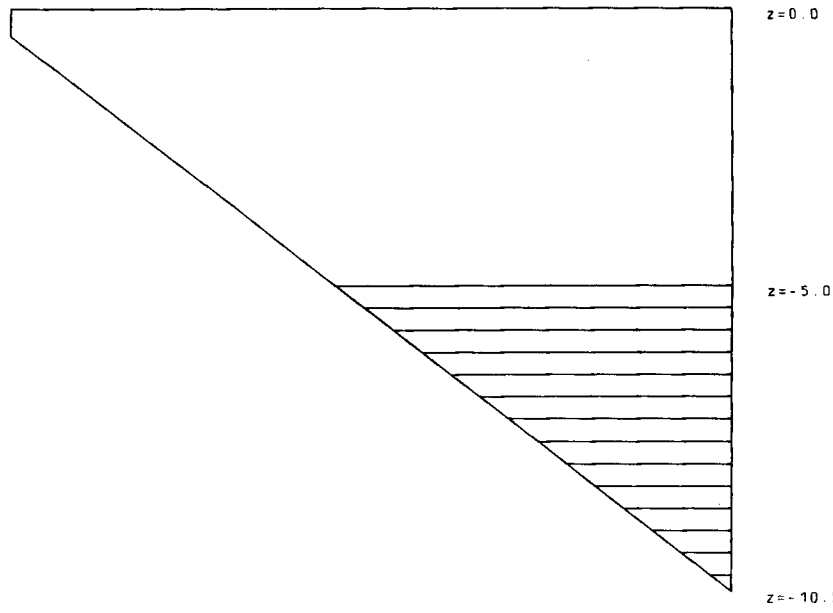

Figure 8. Test problem with trivial solution: zero flow and $c = 0 | z \geqslant -5$, $c = 30 | z < -5$

taken from the steady state solution. Owing to truncation errors in the approximation of the horizontal gradients on the sigma grid, this initial condition is not a steady state solution of the difference equations. The method we propose in this paper gives a steady state solution that is slightly diffused in the vertical direction. Figure 9 shows concentation profiles in the vertical direction of a steady state solution. Many numerical approximations have no steady state solution for this problem, because the truncation errors are never eliminated. If the number of vertical grid points is increased, then the steady state solution becomes more accurate (see Figure 10). For this solution the number of vertical grid points was 80. The number of horizontal grid points was not changed.

This test illustrates that improved stratification is obtained as a result of increasing the vertical resolution without increasing the horizontal resolution. This is contrary to other methods.[9] Figure 11 shows results for a bottom profile with a steeper slope. For such a topography our method introduces only a small amount of numerical vertical diffusion until a steady state is reached.

The second test problem consists of a coupled flow and transport problem. The bathymetry is the same as for the previous test problem but with a steep slope, i.e. the depth $d(x)$ is given by

$$d(x) = \begin{cases} 0{\cdot}5, & 0 \leqslant x < 0, \\ 0{\cdot}5 + (x - 40)/2, & 40 \leqslant x \leqslant 60, \\ 10{\cdot}5, & 60 < x \leqslant 100. \end{cases}$$

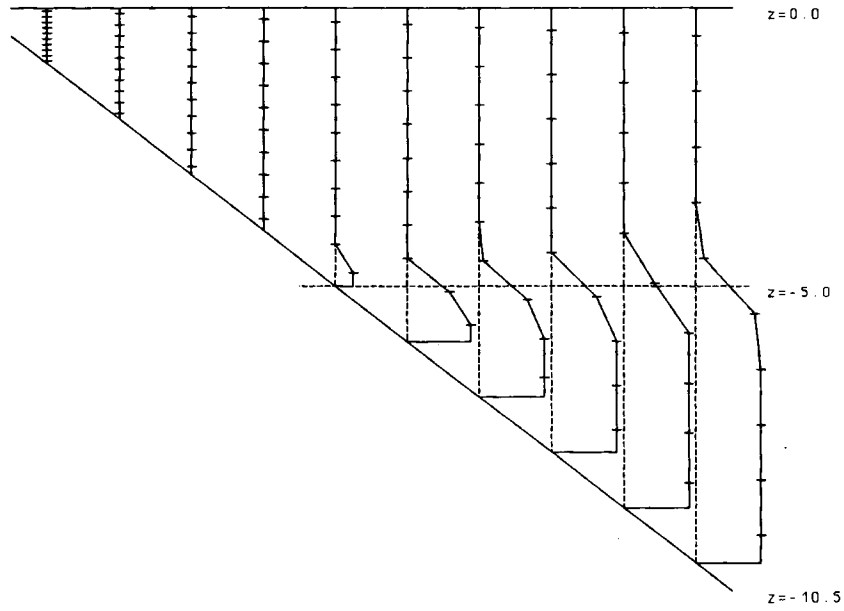

Figure 9. Steady state vertical salinity distribution ($K = 10$)

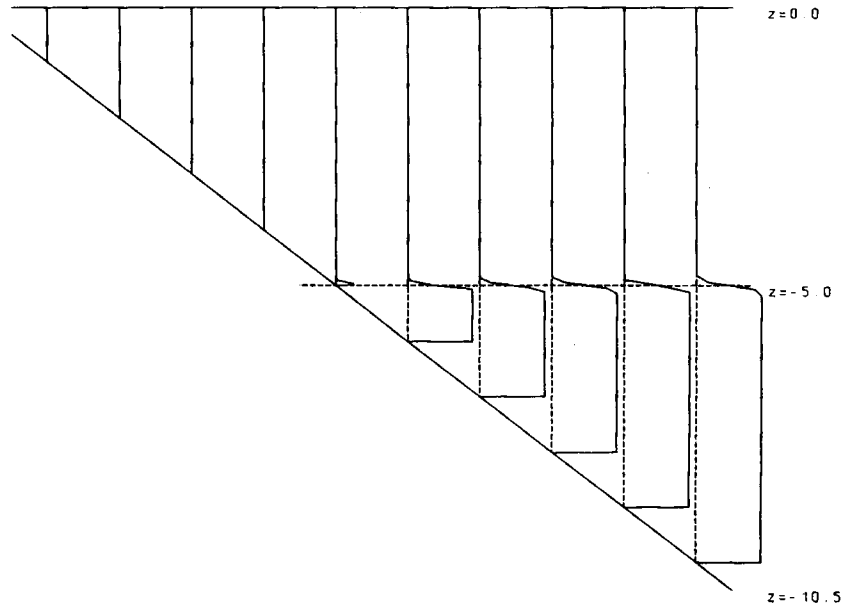

Figure 10. Steady state vertical salinity distribution ($K = 80$)

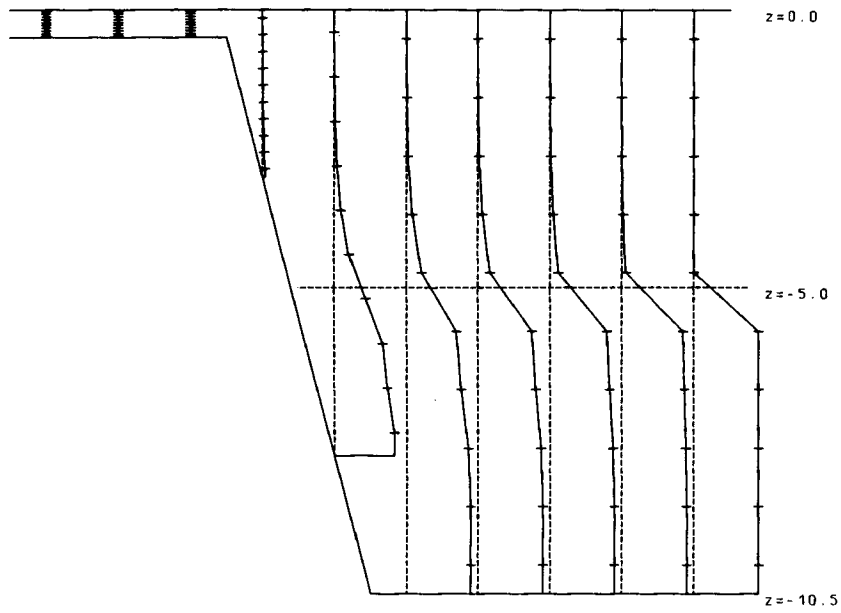

Figure 11. Steady state vertical salinity distribution near steep slope

The system of equations to be approximated is as follows:

$$\frac{\partial u}{\partial t^*} + \frac{1}{\rho_0}\frac{\partial p}{\partial x} = \frac{\nu_v}{H^2}\frac{\partial^2 u}{\partial \sigma^2} + \nu_H \frac{\partial^2 u}{\partial x^{*2}},$$

$$\frac{\partial \zeta}{\partial t^*} + \frac{\partial (Hu)}{\partial x^*} + \frac{\partial \omega}{\partial \sigma} = 0,$$

$$\frac{\partial (Hc)}{\partial t^*} + \frac{\partial (Huc)}{\partial x^*} + \frac{\partial \omega c}{\partial \sigma} = \frac{\partial}{\partial x}\left(HD_H \frac{\partial c}{\partial x}\right).$$

An asterisk indicates that the term is already transformed to the new sigma co-ordinate system. The unmarked terms are still in the Cartesian co-ordinate system. Their transformation takes place implicitly via the numerical method which is used. For the computation of the density a simplified equation of state is used given by

$$\rho = 1000 + c.$$

Zero water levels and velocities are prescribed as initial conditions. The initial condition of the salinity is the same as for the previous test problem. Boundary conditions are given by

$$\frac{\partial c}{\partial x} = 0, \qquad x = 0, \qquad -d(0) \leqslant z \leqslant \zeta(0),$$

$$c(100, z, t) = \begin{cases} 30\,\mathrm{kg\,m^{-3}}, & -d(100) \leqslant z \leqslant 5, \\ 0\,\mathrm{kg\,m^{-3}}, & 5 < z \leqslant \zeta(100). \end{cases}$$

The exchange coefficients D_H and $\nu_{H,V}$ are constant and equal to 10·0, 2·0 and 0·1 $m^2 s^{-1}$ respectively. The vertical diffusion coefficient D_V is set to zero. The exact solution is a trivial one with zero velocities, zero gradients of the water level and a distribution of the salinity equal to the distribution of the previous test problem. Many numerical methods, however, will produce artificial flow for this and similar situations (see e.g. Reference 15). To illustrate this, we first consider an approximation of the pressure term which is based upon a straightforward transformation of the pressure gradient. This straightforward transformation is given by

$$\frac{\partial p}{\partial x} = \frac{\partial p}{\partial x^*} + \frac{\partial \sigma}{\partial x}\frac{\partial p}{\partial \sigma} = \frac{\partial}{\partial x^*} gH \int_\sigma^0 \rho \, d\sigma' + \rho g\left(\frac{\partial \zeta}{\partial x} + \sigma \frac{\partial H}{\partial x}\right).$$

Streamlines for the steady state solution are shown in Figure 12. The maximum velocity obtained near the slope is of the order of 0·15 m s^{-1}. This is entirely due to truncation errors! The concentration profiles are shown in Figure 13.

Our method produces initially some artificial flow until the concentration field has reached a steady state. The velocities are decreased by vertical viscosity and bottom friction. In the steady state the velocities are absolutely zero. The concentration distribution is shown in Figure 14.

It should be noted that the equilibrium solution is independent of the amount of horizontal eddy diffusivity as long as the coefficient is not zero. To reach the steady state solution as fast as possible, it is efficient to start the computations initially without density effects in the pressure term, the so-called diagnostic mode,[16] and then to continue with density effects, the so-called prognostic mode.[16]

The third test is a three-dimensional diffusion problem. The bathymetry is shown in Figure 15. It has different bottom slopes in different directions. The basin is closed at all boundaries. This means that zero fluxes are prescribed at all boundaries. The computational domain consists of 10 × 10 × 10 grid points. The initial conditions are the same as for the first test problem. The steady state solution is shown in Figure 16. All diffusive fluxes are approximately zero, i.e. the flow generated by density differences will be zero too for this case.

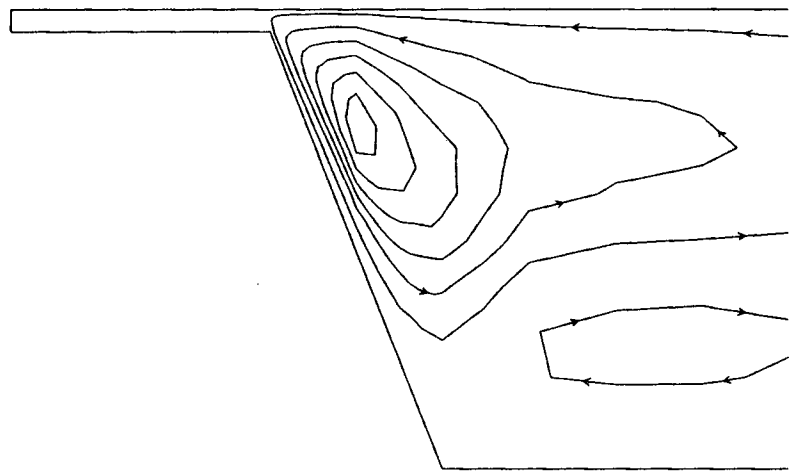

Figure 12. Flow due to truncation errors

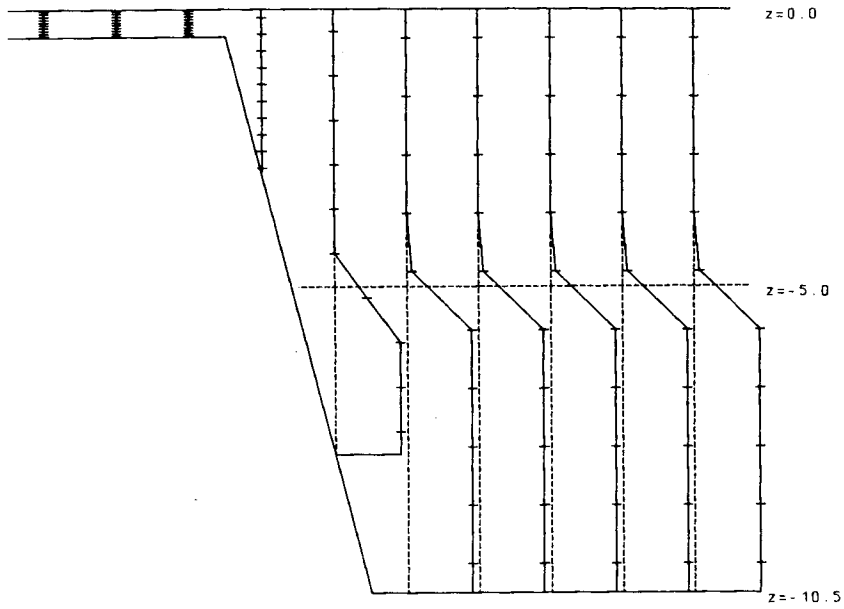

Figure 13. Vertical salinity distribution ($K = 10$), Dirichlet boundary condition

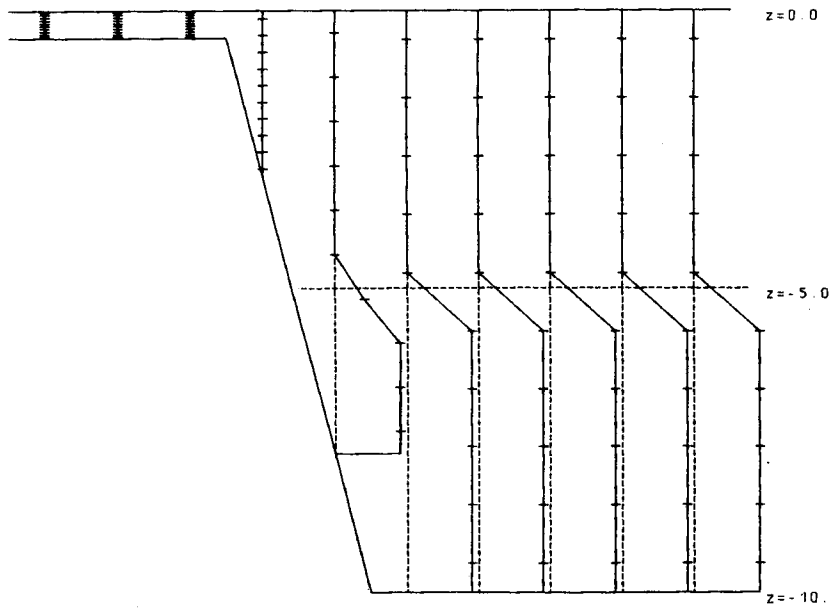

Figure 14. Concentration profiles of steady state solution

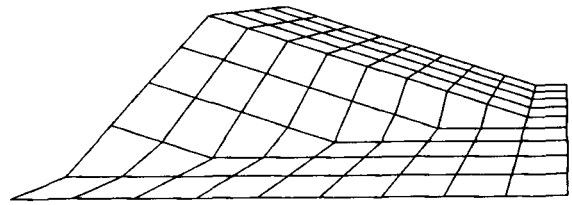

Figure 15. Bathymetry of 3D test problem

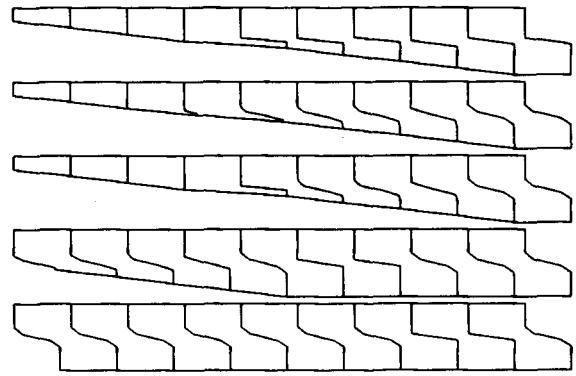

Figure 16. Concentration profiles in various cross-sections

It should be noted that if Dirichlet-type boundary conditions are prescribed (i.e. concentrations), then zero fluxes are not always the steady state equilibrium solution, despite the fact that this might well be the case for the solution of the differential equations. Hence artificial flow might remain. This artifical flow will in general be small, but if this hampers the accuracy significantly, then concentrations can be compared firstly on the basis of purely von Neumann (flux) boundary conditions. Boundary conditions derived from the steady state solution can be prescribed with a slightly diffused vertical concentration gradient, so that in the case of a steady state solution all fluxes are zero. Hence in the prognostic mode artificial flow will not be generated.

6. CONCLUDING REMARKS

In this paper a numerical method has been derived for the approximation of horizontal gradients in sigma co-ordinates which does not introduce large truncation errors in the case of vertical stratification. For the approximation of the horizontal diffusive fluxes this method is based upon a finite volume approach. This allows derivation of the method conceptually within Cartesian co-ordinates although a sigma grid is used. Owing to a simple filter that does not influence the consistency, the method is positive and does not have truncation errors that produce artificial vertical diffusion.

When the computation of the horizontal pressure gradient is based upon integration of the horizontal concentration gradients as computed with the transport algorithm, then artificial upwelling is minimized. The set-up of an additional Cartesian grid increases the computational complexity. However, the increase in computational cost is relatively small.

When this approach is used, sigma co-ordinate systems can be applied to simulations of

stratified flow in estuaries with tidal flats and steep bottom slopes, even in cases where the 'hydrostatic consistency' condition is violated.

REFERENCES

1. R. L. Haney, 'On the pressure gradient force over steep topography in sigma coordinate ocean models', *J Phys. Oceanogr.*, **21**, 610–619 (1991).
2. J. J. Leendertse, 'Turbulence modelling of surface water flow and transport: Part IIIa', *J. Hydraul. Eng.*, **116**, 600–607 (1990).
3. K. Dyer, *Estuaries: A Physical Introduction*, Wiley, New York, 1973.
4. N. A. Phillips, 'A coordinate system having some special advantages for numerical forecasting', *J Meteorol.*, **14**, 184–185 (1957).
5. E. Deleersnijder and J. M. Beckers, 'On the use of the σ coordinate system in regions of large bathymetric variations', *J. Marine Syst.*, **3**, 381–390 (1992).
6. G. L. Mellor and A. F. Blumberg, 'Modelling vertical and horizontal diffusivities with the sigma co-ordinate system', *Mon. Weather Rev.*, **113**, 1379–1383 (1985).
7. J. M. Gary, 'Estimate of truncation error in transformed primitive equation atmospheric models', **30**, 223)233 (1973).
8. Z. I. Janjić, 'Pressure gradient force and advection scheme used for forecasting with steep and small scale topography', *Beitr. Phys. Atmos.*, **50**, 186–199 (1977).
9. F. Mesinger and Z. I. Janjić, 'Problems and numerical methods in the incorporation of mountains in atmospheric models', in *Lectures in Applied Mathematics*, Vol. 22, Springer, New York, 1985, pp. 81–120.
10. R. Peyret and T. D. Taylor, *Computational Methods for Fluid Flow*, Springer, New York, 1983.
11. C. A. J. Fletcher, *Computational Techniques for Fluid Dynamics*, Vol I and II, Springer, New York, 1989.
12. C. Hirsch, *Numerical Computation of Internal and External Flows*, Wiley, New York, 1990.
13. J. D. Lambert, *Numerical Methods for Ordinary Differential Systems*, Wiley, New York, 1991.
14. D. Greenspan and V. Casulli, *Numerical Analysis for Applied Mathematics, Science and Engineering*, Addison-Wesley, Reading, MA, 1988.
15. F. Mesinger, 'On the convergence and error problems of the calculation of the pressure gradient force in sigma coordinate models,' *Geophys. Astrophys. Fluid Dyn.*, **19**, 105–117 (1982).
16. A. F. Blumberg and G. L. Mellor, 'Diagnostic and prognostic numerical circulation studies of the South Atlantic Bight,' *J. Geophys. Res.*, **88**, 4579–4592 (1983).